Spray-Drying Process Optimization and Modeling for an Inhaled Dry Powder of 5-Azacytidine for Treating Local and Metastatic Lung Cancer

Rebekah M. Anderson, Steven A. Belinsky, Lindsey M. Earnest, Philip J. Kuehl, Christian Luebbert, Conor A. Ruzycki, David T. Vodak, and Michael E. Grass*



Downloaded via Michael Grass on November 12, 2025 at 16:27:35 (UTC). See https://pubs.acs.org/sharingguidelines for options on how to legitimately share published articles.

Cite This: https://doi.org/10.1021/acs.molpharmaceut.5c00799



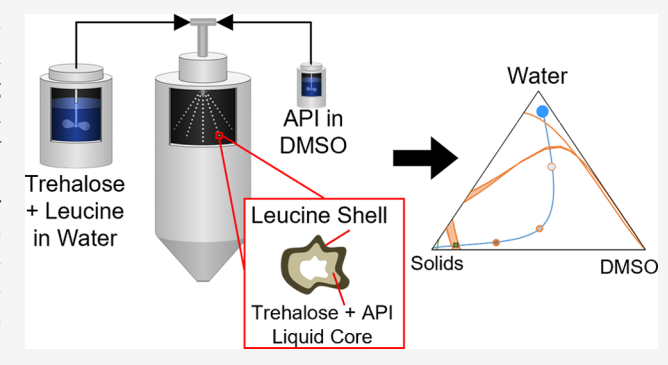
ACCESS I

III Metrics & More

Article Recommendations

s Supporting Information

ABSTRACT: A spray-dried powder formulation of 5-azacytidine (5-AZA) recently showed significantly improved tumor reduction and systemic exposure for the potential treatment of metastatic lung cancer. To support clinical use, the target product profile required double the active loading. Here, a series of powders were spray dried to increase 5-AZA loading in the formulation, and process parameters were varied to identify variables controlling powder properties. Formulations were sprayed via in-line mixing, where separate dimethyl sulfoxide (DMSO) and aqueous solutions were mixed immediately upstream of atomization. A core—shell structure was observed matching previous reports of spray-dried L-leucine with sugar from water and ethanol. To the best of our knowledge, this is the first study investigating the process and structure of



spray-dried L-leucine and trehalose using DMSO and water as processing solvents. Powders with glass transition temperatures $(T_{\rm g})$ below room temperature were successfully manufactured with high yields, attributed to the crystalline L-leucine shell surrounding the low $T_{\rm g}$ core. The residual DMSO was controlled by the DMSO:water ratio and the composition of the core. Perturbed-Chain Statistical Associating Fluid Theory (PC-SAFT) was employed to understand droplet drying processes by developing ternary phase diagrams and drying trajectories. This work enables the manufacture of both dry inhalable 5-AZA powder for the treatment of lung cancer and low $T_{\rm g}$ materials previously thought to be unmanufacturable via spray drying. It also highlights the importance of aligning experimental data and theoretical models to improve our understanding of complex processes.

KEYWORDS: spray drying, particle engineering, PC-SAFT, inhalation

INTRODUCTION

5-Azacytidine (5-AZA) is a known therapeutic that acts via cytosine DNA-methyltransferase inhibition in cancer therapy. 1-3 Due to its mechanism of action and the hundreds of genes with cytosine methylated promoter regions associated with reduced transcription in non-small cell lung cancer (NSCLC), ⁴ 5-AZA has been evaluated in both preclinical and clinical studies as a therapeutic for NSCLC as a nebulized and dry powder formulation with positive results.⁵ Inhaled delivery of 5-AZA allows for direct deposition and absorption, avoiding hepatic first-pass metabolism and gastrointestinal toxicity observed in oral formulations.^{6–8} A major limitation for lung delivery of 5-AZA, and therefore reproducible efficacy, is the ability to achieve higher doses with reproducible deposition in the target areas of the lung. Previous studies have shown that a nebulized form can be efficacious, but the long duration of treatment (approximately 90 min) and the lack of sufficient systemic exposure aimed at treating metastatic disease are limiting. 9,10 Recently, an engineered particle formulation was

developed and tested in an orthotopic rat model in comparison with a nebulized form. The 10/20/70 5-AZA/L-leucine/trehalose (w/w) engineered dry particle formulation, prepared by spray drying, showed significantly improved tumor reduction and systemic exposure compared to inhaled aqueous and injected formulations.

Particle engineering by spray drying allows for tunability of key pulmonary powder properties including particle size, density, and particle structure, targeting aerodynamic diameters between approximately 1 and 5 μ m. Formulations of spray-dried powders comprised of trehalose and L-leucine have been well-documented in the literature to form

Received: May 30, 2025 Revised: October 29, 2025 Accepted: October 29, 2025



Molecular Pharmaceutics pubs.acs.org/molecularpharmaceutics

Figure 1. Schematic of the in-line mixing spray-drying process used and a conceptual rendering of the droplet drying trajectory.

dispersible respirable powders with a core—shell architecture. 14,15 In these studies, L-leucine is observed to accumulate at the surface of the droplet during the early stages of evaporation, while the trehalose solidifies to a glass with a high glass transition temperature $(T_{\rm g})$ in the core to stabilize the active molecule in the formulation. 15,16 The resulting particle structure features a corrugated crystalline L-leucine shell, which reduces to reduce particle agglomeration and improve dispersibility. $^{17-19}$ This platform architecture has enabled many formulations for dry powder aerosols. 20

The majority of this core-shell platform work has been done using either water or ethanol:water blends as processing solvents. 16,20 Although 5-AZA, L-leucine, and trehalose are sufficiently soluble in water to prepare spray solutions, 5-AZA rapidly hydrolyzes in aqueous media²¹ and is insoluble in ethanol and other highly volatile spray-drying solvents.²² To enable spray drying of the 10/20/70 5-AZA/L-leucine/ trehalose formulation and prevent degradation during processing, an in-line mixing process was developed where 5-AZA is dissolved in dimethyl sulfoxide (DMSO) and then mixed with an aqueous solution of L-leucine and trehalose directly prior to atomization (Figure 1).8 To our knowledge, the work by Kuehl et al. is the only example of using a DMSO/ water solvent system aimed at achieving this core-shell architecture. That publication did not elaborate on the process or physical properties of the material..8 Upon characterization of the produced formulation, the resulting powder contained approximately 10 wt % residual DMSO.8 The dry powder demonstrated significantly improved pharmacokinetics and efficacy in the in vivo model with a reduced dose (0.6 mg/kg lung dose vs systemic 2 mg/kg, i.p.). The authors hypothesized that the residual DMSO increased absorption and systemic exposure.²³

The goals of this work were two-fold: (1) increase loading of 5-AZA from 10 to 20 wt % while maintaining or improving powder properties and (2) demonstrate tunability for residual DMSO in the spray-dried powder. The drug loading was set to 20% based on a target clinical dose determined based on available systemic dosing of 5-AZA in humans and preclinical studies comparing IV and inhaled 5-AZA. L-Leucine was maintained at 20% based on previous work, demonstrating that

this L-leucine concentration provides a robust core—shell architecture. Tunability of DMSO is important because the previous work demonstrated significantly more tumor reduction from the DMSO-containing dry powder relative to aqueous-only nebulization, while DMSO may decrease the physical stability of the DPI.

A series of spray-dried powders were manufactured via inline mixing with 10 and 20 wt % 5-AZA while varying spraydrying process parameters (5-AZA loading in DMSO, water:DMSO feed ratio, etc.). This process includes three solid components and two solvents (water and DMSO) with distinct heats of vaporization during the spray-drying process. We employed a Perturbed-Chain Statistical Associating Fluid Theory (PC-SAFT) model to better understand this complicated process and the variables available for optimization. PC-SAFT has been extensively used to model the thermodynamic behavior of complex mixtures in pharmaceutical formulations. In recent years, PC-SAFT has found numerous applications in predicting phase equilibria, shelf life stability, and processing conditions for drug formulations, particularly in amorphous solid dispersions (ASDs). By accurately predicting the interactions among active pharmaceutical ingredients (APIs), excipients, and solvents, PC-SAFT provides a robust framework for optimizing manufacturing processes such as spray drying. Recent studies have applied PC-SAFT to simulate the drying trajectories in ASDs, guiding the design of phase diagrams that account for solvent evaporation and miscibility gaps. PC-SAFT allows for the prediction of drying curves, miscible regions, and glass transition temperatures, which are critical in designing stable, homogeneous formulations. Dohrn et al. successfully modeled the phase separation of HPMCAS and naproxen during spray drying to avoid unwanted crystallization and phase separation. 24,25 This was ultimately applied to modeling the process space of spray drying.26

Here, PC-SAFT was used to develop ternary phase diagrams and model the composition of the droplet as a function of drying progress, including the various phase transitions that occur during evaporation of the solvent blend. The PC-SAFT model in combination with experimental data suggests that this formulation and process would not be feasible without L-

Table 1. Spray-Drying Solution Compositions, Solution Feed Ratios, and Yield

sample ID	92-1	93-1	93-2	93-3	93-4	65-1	66-1
solids composition (w/w, 5-AZA/trehalose/leucine)	10/70/20	20/60/20	20/60/20	20/60/20	20/60/20	0/78/22	0/100/0
water:DMSO feed ratio (wt/wt %)	90/10	92.4/7.6	90/10	80/20	95.2/4.8	90/10	90/10
total solids loading (wt %)	5	1.9	5	5	2.4	4.5	4.5
DMSO phase solids loading (wt %)	5	5	10	5	10	0	0
aqueous phase solids loading (wt %)	5.0	1.6	4.5	5.0	2.0	5.0	5.0
aqueous phase solids composition (trehalose/L-leucine, wt/wt %)	78/22	75/25	75/25	75/25	75/25	78/22	100/0
yield (%)	74	76	92	86	87	87	6

leucine functioning as a hard, protective shell that prevents the plasticized core (comprising 5-AZA/trehalose/DMSO/water) from agglomerating or "spray painting" the spray dryer chamber during processing. In addition to the well-known functionality of L-leucine as a powder dispersal enhancer, this study demonstrated that the phase behavior of L-leucine in the DMSO/water system can also function as a barrier to protect against coalescence of a more liquid core during processing.

MATERIALS AND METHODS

Spray-Dried Powder (SDP) Preparation. Based on previous work, the hydrolytic degradation of 5-AZA in aqueous media led to evaluation of other solvent systems and DMSO was selected as the solvent for 5-AZA dissolution. Therefore, here, two solutions were prepared for each batch: an aqueous solution and a DSMO solution. L-Leucine (Cat. No. MACR4944-06, Avantor/VWR, Pennsylvania, USA) and a, atrehalose dihydrate (Cat. No. T-104–4-IG-RD, Pfanstiehl Inc., Illinois, USA) were dissolved in ultrapure water. 5-Azacytidine (5-AZA, provided by Lovelace Biomedical) was dissolved in dimethyl sulfoxide (Cat. No. 9033-33, VWR, Pennsylvania, USA). Solutions were stirred until all solids were dissolved. See Table 1 for the spray solution compositions.

The solutions were spray dried using a custom feasibility-scale spray dryer with a 40 kg/h drying gas capacity (SD-40). The SD-40 was operated in an open loop (single pass) configuration with a Spraying Systems 1/4J Series 1650LC—64AC external mixing two-fluid nozzle. The two solutions (aqueous and DMSO) were fed to the SD-40 via in-line mixing configuration (Figure 1), mixing immediately upstream of the nozzle. Powders were manufactured with nitrogen drying gas flow rates of 497–502 g/min, atomization pressures of 59–61 psig, a total solution flow rate of 8.0 g/min, outlet temperatures of 69–71 °C, and inlet temperatures of 133–145 °C. Refer to Table S1 in the Supporting Information for the spray-drying process averages. Following SDP manufacture, powders were stored in sealed amber glass jars at 2–8 °C.

Scanning Electron Microscopy (SEM). The surface morphology of the SDPs was analyzed via scanning electron microscopy. SEM samples were prepared by dry depositing powder on a 1 × 1 cm Si coupon. Images were then acquired on a ThermoFisher Apreo 2S Lo, using Optiplan imaging mode at 1 kV, with a 500 V stage bias.

X-ray Diffraction (XRD). X-ray diffraction was performed using a Miniflex 6G Diffractometer (Rigaku, Tokyo, Japan) with a D/tex Ultra detector. Samples were prepared on a Si510 low background sample holder and analyzed with a 2θ range of $3-40^{\circ}$ and a scan rate of 2.5° /min. The resultant diffraction patterns were then evaluated for signs of crystallization and compared to the diffraction patterns of the raw materials.

Particle Size Distribution (PSD). The geometric particle size distribution (PSD) was determined via a dry dispersion

method on a Helos laser diffraction system (Sympatec, Clausthal-Zellerfeld, Germany). Samples were dispersed using the RODOS/L disperser type at a primary pressure of 0.5 bar and trigger of \geq 1% C_{opt}. The R2 lens (0.25/0.45–87.5 μ m measuring range) was used to measure each sample. Particle size was then calculated by Fraunhofer theory in PAQXOS 6.0.1 software (Sympatec GmbH). Each sample was analyzed in triplicate.

Differential Scanning Calorimetry (DSC). Spray-dried powder samples were prepared in triplicate by weighing 2–10 mg of powder and placing them in Tzero pans (Part No. 901683.901, TA Instruments, DE, USA). Tzero hermetic lids (Part No. 901684.901, TA Instruments, DE, USA) were hermetically sealed to the pans, and samples were loaded into a Discovery X3 Differential Scanning Calorimeter (TA Instruments, DE, USA). Modulated DSC (mDSC) was performed by equilibrating samples at –40 °C, modulating the temperature 1.5 °C for 60 s, and then ramping 2.5 °C/min to 100–120 °C. Data was analyzed using TRIOS 5.8.1.14 software (TA Instruments, DE, USA).

Karl Fischer Titration (KF). Water content of the manufactured powders was analyzed with a C30S Coulometer Karl Fischer Titrator (Mettler Toledo, OH, USA) and InMotion KF oven autosampler. Powder samples, standards, and atmospheric blanks were prepared in triplicate. Powder and standard samples were prepared by weighing approximately 50 mg of powder and sealing them inside a glass KF vial. KF was performed with a sample temperature of 130 °C and a standard temperature of 150 °C. The water mass from atmospheric blanks was subtracted from those of powder and standard samples.

Gas Chromatography (GC). The residual DMSO content of the manufactured powders was analyzed by headspace GC using an Agilent 8890 Gas Chromatograph and an Agilent 7697C headspace sampler (Agilent, CA, USA) with a Phenomenex ZB-WAX column and FID detector. A calibration curve was prepared using 1,3-dimethyl-2-imidazolidinone (DMI) as a dilution solvent with a concentration range of 750–10,500 ppm for DMSO. SDP samples were prepared by dissolving the SDP (10 wt %) in DMI. Reference Table S2 in the Supporting Information for GC method details.

High-Performance Liquid Chromatography (HPLC). Determination of 5-AZA content and quantification of related substances of the spray-dried powders was completed via HPLC (Agilent 1260 Infinity II HPLC) using diluent (10 g/L sodium bisulfite in water, pH adjusted to 2.5 with dilute sulfuric acid), mobile phase A (1.54 g/mL ammonium acetate in water), and mobile phase B (20:30:50 acetonitrile:methanol:mobile phase A). Working standard solutions were prepared by dissolving 20 mg of 5-AZA into 10 mL of diluent. Limit of quantification (LOQ) solutions were prepared by adding 0.5 mL of working standard solution to 99.5 mL of

diluent. The sample solutions were 2 mg/mL 5-AZA in the diluent. The column (Phenomenex Luna 5 μ m C18 (2) 100 Å, 4.6 mm \times 25 cm) was operated at 5 °C with a flow rate of 0.8 mL/min and a 270 nm UV detector. The injection volume was 5 μ L and the data acquisition time was 50 min. Reference Table S3 in the Supporting Information for HPLC gradient parameters.

PC-SAFT Calculations. The Perturbed-Chain Statistical Associating Fluid Theory (PC-SAFT) is a widely used thermodynamic model for predicting phase behavior in complex mixtures, including solvent evaporation and drying processes. PC-SAFT was applied in this study to understand the spray-drying process for optimizing a dry powder formulation containing trehalose, L-leucine, and 5-AZA using Solcalc (Amofor GmbH, Dortmund, Germany). The model accurately predicts phase equilibria and drying curves for the ternary and quaternary systems encountered in pharmaceutical formulations, including nonideal behaviors such as miscibility gaps, glass transition, and crystallization.

PC-SAFT models the Helmholtz free energy by considering three primary contributions: the hard-chain term (for molecular size and shape), the dispersion term (for van der Waals forces), and the association term (for hydrogen bonding). The residual Helmholtz energy $a_{\rm res}$ is expressed as

$$a_{\rm res} = a_{\rm hc} + a_{\rm disp} + a_{\rm assoc}$$

Here, $a_{\rm hc}$ represents the hard-chain contribution accounting for the chain length and segment diameter, $a_{\rm disp}$ handles attractive forces between the molecules, and $a_{\rm assoc}$ describes the energy contribution from association interactions, such as hydrogen bonds.

Equilibrium between Vapor Phase and Droplet (VLE) and Demixing (LLE). To describe the equilibrium between the vapor and liquid phases during solvent evaporation, the following vapor—liquid equilibrium (VLE) conditions are used:

$$\gamma_i^{\mathrm{L}} x_i^{\mathrm{L}} p_i^{\mathrm{sat}} = y_i p$$

where γ_i^L is the activity coefficient of component i in the liquid phase, x_i^L is the mole fraction of i in the liquid phase, p_i^{sat} is the saturation pressure of component i, and y_i is the mole fraction of i in the vapor phase at pressure p.

The drying trajectory is modeled through iterative VLE calculations, where the composition of the liquid phase changes as the solvent evaporates. If phase separation occurs (i.e., a miscibility gap is crossed), then the system splits into two coexisting liquid phases. This can be mathematically represented by the following set of equations for component *i* between two liquid phases L1 and L2:

$$\gamma_i^{\mathrm{L1}} x_i^{\mathrm{L1}} = \gamma_i^{\mathrm{L2}} x_i^{\mathrm{L2}}$$

Prediction of Drying Trajectories. In spray drying, solvent evaporation leads to progressive changes in the mixture's composition. PC-SAFT can predict these drying trajectories by computing the evolving liquid-phase composition and identifying phase boundaries, such as miscibility gaps and glass transition temperatures. For ternary and quaternary systems, phase diagrams are constructed, showing the path of the drying curve and potential phase transitions. For example, in the current study involving a solvent mixture of DMSO and water, the drying trajectory was predicted to

remain in the homogeneous region for specific compositions, avoiding unwanted liquid—liquid phase separation.

At each step of the drying process, the following solvent balance is maintained:

$$n_{\text{liquid}} = n_{\text{initial}} - n_{\text{vapor}}$$

where n_{liquid} and n_{vapor} are the amounts of solvent in the liquid and vapor phases, respectively. The drying continues until the desired residual solvent content is reached, at which point the final powder is collected.

Shell Formation—Solubility Prediction of Crystalline Components. The solubility of a crystalline component, such as a supersaturated API or a crystallizing excipient such as Lleucine, in a solvent or a solvent—polymer mixture can be predicted using the solid—liquid equilibrium (SLE) condition. In PC-SAFT, this equilibrium is achieved when the chemical potential of the component in the crystalline (solid) phase is equal to that in the liquid phase. The general expression for the solubility of a crystalline component is given by the following equation:

$$\ln x_i = \frac{\Delta H_{\rm m}}{R} \left(\frac{1}{T_{\rm m}} - \frac{1}{T} \right) + \frac{\Delta C_{\rm p}}{R} \left[1 - \frac{T}{T_{\rm m}} + \ln \left(\frac{T}{T_{\rm m}} \right) \right] + \ln \gamma_i$$

where x_i is the mole fraction of the crystalline component in the liquid phase (solubility), $\Delta H_{\rm m}$ is the melting enthalpy of the crystalline material, $\Delta C_{\rm p}$ is the difference in the heat capacities between the liquid and solid phases, $T_{\rm m}$ is the melting temperature of the crystalline component, T is the temperature at which the solubility is being calculated, and R is the universal gas constant. This equation models the temperature dependence of the solubility of crystalline components and includes corrections for nonidealities in the mixture, represented by the activity coefficient γ_i . In cases where the mixture contains solvents, excipients, and polymers, the solubility of a crystallizing component such as L-leucine in the shell can be affected by interactions between all species present in the system, which is captured by PC-SAFT.

During spray drying, L-leucine crystallizes at the particle surface, forming a shell. The properties of the incoming crystalline L-leucine were used in the PC-SAFT calculations because the thermodynamic properties of spray-dried L-leucine are not well-described. The onset of crystallization is determined by the solubility limit predicted by the above equation. Once the concentration of leucine in the liquid phase exceeds the solubility, crystallization will occur, leading to the formation of the shell. The drying trajectory, as calculated by PC-SAFT, helps identify when and where this supersaturation and subsequent crystallization occur during the drying process.

By combining evaporation, crystallization, and demixing with PC-SAFT and a mass balance, it becomes possible to predict the drying trajectory, shell formation (amount of crystalline material relative to the amorphous core), and residual solvent content.

RESULTS

Properties of Formulation Components. 5-AZA is known to rapidly chemically degrade in aqueous media where it is reported that over 20 wt % is hydrolyzed within an hour of media exposure. S-AZA is soluble and chemically stable in DMSO, and therefore a DMSO solution was used here to

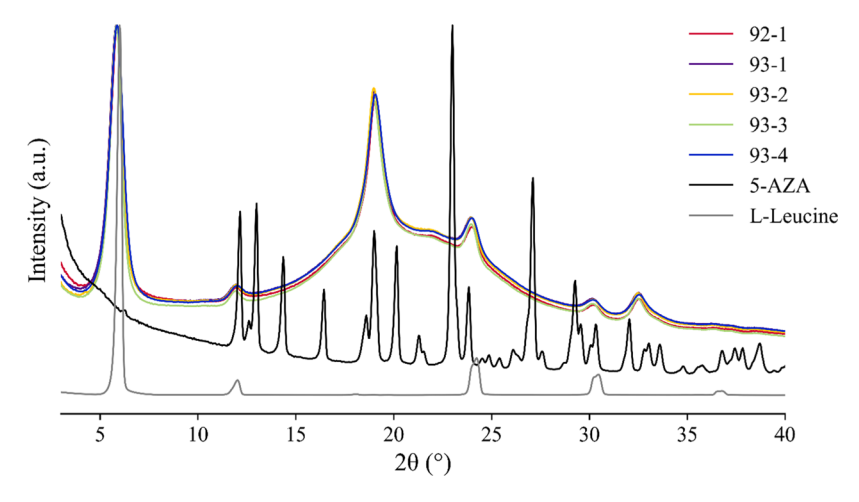


Figure 2. Diffraction patterns of spray-dried powders compared to as-received 5-AZA and L-leucine.

Table 2. Geometric Particle Size Distribution for All Manufactured Powders

sample ID	92-1	93-1	93-2	93-3	93-4	65-1	66-1
mean d_{10} (μ m)	0.67 ± 0.02	0.56 ± 0.01	0.63 ± 0.02	0.61 ± 0.01	0.57 ± 0.04	0.55 ± 0.03	1.53 ± 0.03
mean d_{50} (μ m)	2.46 ± 0.06	1.83 ± 0.02	2.51 ± 0.04	2.58 ± 0.02	2.03 ± 0.05	2.38 ± 0.08	6.55 ± 0.26
mean d_{90} (μ m)	5.04 ± 0.05	3.73 ± 0.02	5.04 ± 0.05	5.18 ± 0.02	4.05 ± 0.02	5.98 ± 0.14	27.26 ± 0.63
mean SMD (μm)	1.54 ± 0.03	1.25 ± 0.02	1.52 ± 0.03	1.51 ± 0.01	1.31 ± 0.05	1.39 ± 0.06	3.14 ± 1.94

Table 3. Compositional Analysis for Powders Containing 5-AZA

sample ID	92-1	93-1	93-2	93-3	93-4
water (wt %)	2.25 ± 0.03	3.01 ± 0.07	2.41 ± 0.03	2.61 ± 0.06	2.58 ± 0.05
DMSO (wt %)	10.8	9.1	9.5	12.2	8.3
5-AZA (wt %)	9.7	18.9	18.4	19.3	18.9

dissolve the 5-AZA and limit hydrolysis. L-Leucine and trehalose were dissolved in water. Reference Table S4 in the Supporting Information for physiochemical properties and solubilities of each of the formulation components.

Production of Spray-Dried Powder Formulations. Seven different formulations were spray dried with varying compositions and processing conditions (Table 1). Reference Table S1 in the Supporting Information for the spray-drying manufacturing summary. All batches were executed at an 8 g target batch size using the spray-drying process described in the Methods section. A control formulation (92-1) was produced to match the lead formulation and process that has been previously manufactured. The subsequent 4 SDPs featured increased active loading (20 wt %). The effect of total solids loading and water:DMSO ratio was studied via samples 93-1 through 93-4. The last two SDPs (65-1 and 66-1) were manufactured to evaluate the impact of L-leucine.

Yield was assessed following manufacture of the spray-dried powders. Notably, the yield for the sample without L-leucine (66-1) was significantly lower than that of all other manufactured powders (6% vs 74–92%, respectively).

Characterization of Powders. Characterization of the manufactured spray-dried powders shows particle structure consistent with typical spray-dried trehalose/L-leucine dry powders for inhalation (Figure 2). These materials show diffraction patterns consistent with spray-dried L-leucine. ^{29–33} As observed in other spray-dried powders containing L-leucine, the structure of spray-dried leucine does not match that of the incoming leucine crystal pattern and features broad peaks, including one at approximately 19° 20. ^{34,35} This feature and

other broad peaks observed from spray drying L-leucine have been attributed to formation of a liquid-crystal type structure on the surface of the spray-dried particles.³³ The broad amorphous background is attributed to the amorphous dispersion of 5-AZA and trehalose. Additionally, SEM images show a highly corrugated morphology consistent with inhalation powders prepared by spray drying similar formulations (Figure S1 in the Supporting Information). The particles appear to be porous; however, this is not expected and may result from solvent evacuating particles under a vacuum during imaging.

The geometric particle size distribution (PSD) was analyzed for all manufactured powders (Table 2). For samples containing L-leucine and 5-AZA, the geometric mean (d_{50}) ranges from 1.8 to 2.6 μ m and geometric mean SMD ranges from 1.2 to 1.6 μ m. The 100% trehalose sample (66-1) has a notably larger particle size with a geometric mean of 6.5 μ m and a mean SMD of 3.1 μ m. PSDs for all formulations containing L-leucine do not show signs of particle fusion. While mass mean aerodynamic diameter (MMAD) was not assessed via cascade impaction, a separate lot of the same formulation was assessed via NGI and laser diffraction (data not included), where the MMAD lay within the d_{50} and d_{90} .

Compositional analysis was completed for powders containing 5-AZA (Table 3). The residual water content was determined by KF to be between 2.2 and 3.0 wt %. Residual DMSO content by GC varied between 8.3 and 12.2 wt % for the 5 powders analyzed. The 5-AZA loading in each formulation was on target. No related substances were

Molecular Pharmaceutics

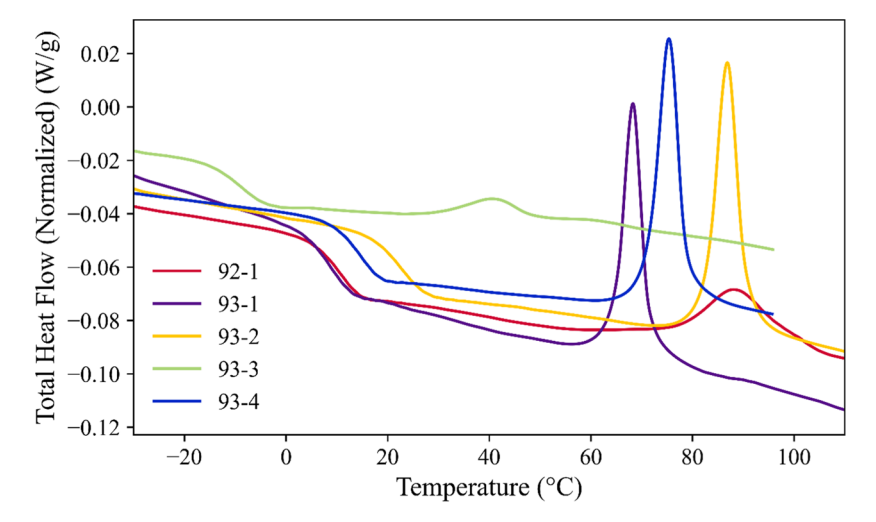


Figure 3. Total heat flow curves for the spray-dried powders. Glass transition events are observed between -6 and 25 °C. Crystallization is observed between 40 and 94 °C.

Table 4. Summary of Thermal Analysis for the As-Manufactured Powders by mDSC

sample ID	92-1	93-1	93-2	93-3	93-4
T _g (°C)	16.7 ± 2.0	12.3 ± 1.3	25.2 ± 1.8	-6.1 ± 3.6	17.8 ± 0.6
enthalpy of crystallization (J/g)	6.2 ± 0.6	12.1 ± 0.5	14.1 ± 0.5	1.9 ± 1.2	13.3 ± 0.2
crystallization peak (°C)	93.9 ± 4.8	68.3 ± 1.9	84.8 ± 1.9	39.4 ± 3.2	74.6 ± 1.0

identified by HPLC, indicating that 5-AZA did not degrade during the manufacturing process.

Thermal analyses of the as-manufactured powders show glass transitions ($T_{\rm g}$) between -6 and 25 °C (Figure 3, Table 4). For each sample, the glass transition event is followed by a crystallization event. After completion of the mDSC experiment, three SDPs (92-1, 93-1, and 93-2) were extracted from their pans and analyzed via XRD to identify which formulation component crystallized during heating (Figure S2 in the Supporting Information). Comparison to diffraction patterns of 5-AZA, L-leucine, and as-manufactured SDPs shows that the source of the exothermic event is 5-AZA crystallization.

DISCUSSION

Characterization of Spray-Dried Powders. Characterization of the as-manufactured powders shows morphology consistent with respirable spray-dried powders possessing a core—shell structure. L-Leucine crystallized into the expected polymorph observed previously when processing out of the more precedented pure water or ethanol/water solvent system. SEM and laser diffraction show the expected respirable particle size of 2–4 μ m particles with the expected morphology of shriveled raisins or mushrooms.

The final compositions of the experimental powders (93-1 through 93-4) contained approximately 20 wt % 5-AZA with approximately 2 wt % residual water and 8–12 wt % residual DMSO. Within the experimental process conditions, dry powders were produced that doubled the active loading (10% to 20%) and matched the physical state and particle size of the material used in the previous preclinical in vivo study.⁸

Modulated Differential Scanning Calorimetry (mDSC) was performed to understand the physical state of the core material. Although models including Gordon—Taylor are commonly employed to predict glass transition temperatures, no calculations of $T_{\rm g}$ s were made in this work due to uncertainty in the composition of the core, which is required to

make a $T_{\rm g}$ estimation. Instead, we experimentally observed via mDSC that the core material (containing a dispersion of trehalose and 5-AZA with residual water and DMSO) was amorphous, as evidenced by the presence of a glass transition event. Due to the relatively high amount of residual DMSO still contained within the particles, the core $T_{\rm g}$ was low. All measured $T_{\rm g}$ s (-6 °C-25 °C) were significantly lower than the outlet temperature of the spray dryer during processing (70 °C).

The spray drying of low T_g materials typically leads to processing challenges, causing poor drying and "spray painting" of the formulation on the walls of the dryer due to the soft and viscous nature of the spray-dried material.³⁶ The glass transition temperature is widely regarded as the most reliable indicator for adhesion potential of spray-dried materials.³⁷ At an outlet temperature greater than 20 $^{\circ}\text{C}$ above the T_{g} , particle adhesion has been observed to cause a paste-like material rather than powder when spray drying low molecular weight sugars and organic acids, leading to poor yields.³⁸⁻⁴¹ Presently, two primary approaches are used to dry low T_g particles: spray freeze-drying, which generally uses operating temperatures below $T_{\rm g}$ + 20 °C and is often not economical, ^{38,42} and the addition of high molecular weight carrier agents such as maltodextrins. During spray drying of fruit juices, high molecular weight additives have been observed to increase the T_g of the product sufficiently for adequate particle collection. ^{39,43} In this work, we present an alternative approach to drying low $T_{\rm g}$ powders via the presence of L-leucine in the formulation. The L-leucine shell is critical to particle formation and the ability to dry and collect soft, viscous, low T_{σ} materials, as exemplified by comparison in yields between sample 66-1 and the rest of the spray-dried powders. We believe this is a novel method to produce low $T_{\rm g}$ spray-dried powders, which can be applied to other drug delivery applications.

Tunability of Residual DMSO Content. With the experiments done in this study, we can identify the processing

Molecular Pharmaceutics

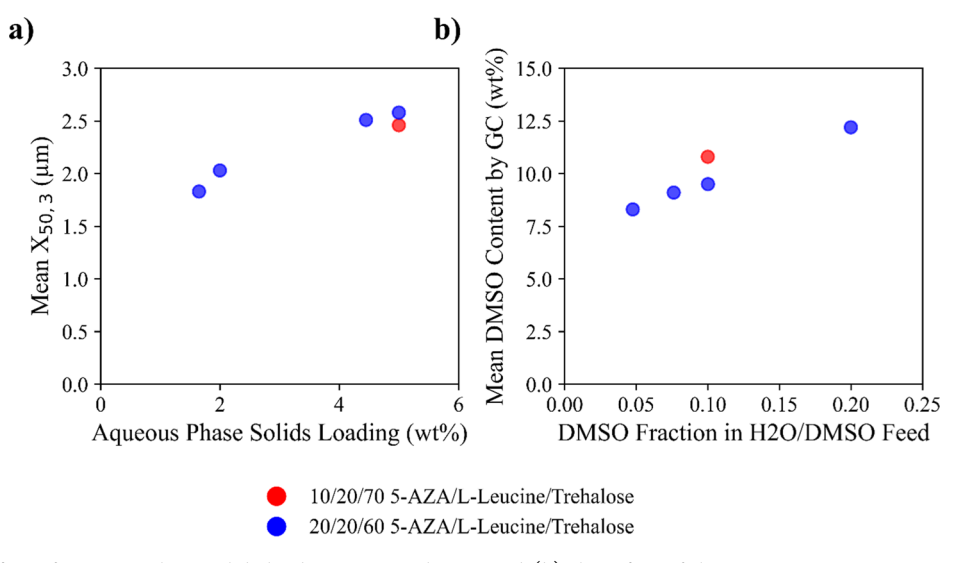


Figure 4. (a) The effect of aqueous phase solids loading on particle size and (b) the effect of the water:DMSO ratio on residual DMSO.

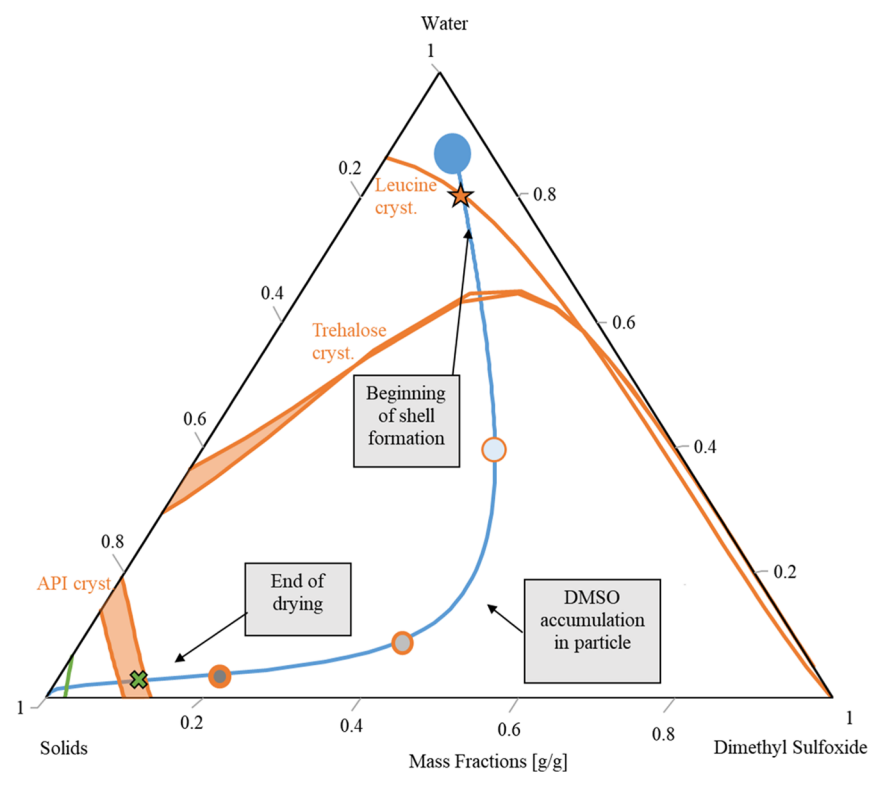


Figure 5. Ternary phase diagram for spray drying of DMSO:water:solids (10/20/70 5-AZA/L-leucine/trehalose) in 90:10 DMSO:water at 70 °C and 5 wt % total solids loading (sample 92-1 conditions). Blue represents predicted droplet composition during drying. Orange represents the crystallization lines of L-leucine, trehalose, and 5-AZA. Green represents the glass transition.

parameters that dictate key quality attributes of the manufactured powders. The geometric particle size is primarily dictated by the solids loading of the aqueous phase and presence of L-leucine as a shell former in the aqueous solution (Figure 4a). The relationship between aqueous phase solids loading and geometric particle size suggests these particles possess a core—shell architecture observed for other systems containing L-leucine. The residual DMSO content of the particles is driven primarily by the DMSO:water ratio and to a lesser extent the 5-AZA:trehalose ratio as shown in Figure 4b. Therefore, adjusting the DMSO:water ratio during processing is an effective way to tune the residual DMSO content in the

final spray-dried powder. The data suggest a proportional relationship of DMSO in spray solution to residual DMSO in the spray-dried powders, regardless of drying kinetics.

The $T_{\rm g}$ of the amorphous core of the particles is sensitive to both residual DMSO and water content as well as the 5-AZA/trehalose ratio. The lowest $T_{\rm g}$ measured was sample 93-3, which had the highest DMSO:water ratio by a significant margin (double that of the control formulation 92-1). The residual water content is likely primarily a function of solid loading, as the spray solution is mostly water. This is supported by sample 93-1 (possessing the second lowest $T_{\rm g}$), which was processed with the most dilute spray solution and has the

highest residual water content. In general, residual DMSO decreases the $T_{\rm g}$. The effect of residual DMSO on product stability was out of the scope of this study and is likely dependent on both the active molecule and the overall composition.

DMSO is currently approved by the FDA as a drug (RIMSO-50) for interstitial cystitis and as an absorption enhancer/excipient. In addition, repeated inhalation exposure of rats to DMSO has been conducted. Male Sprague-Dawley rats were exposed via a nebulizer to 200 mg/m³ DMSO for 7 h a day, 5 days a week, for 6 weeks. 44 All animals showed normal weight gain during exposure, and histopathologic evaluation of organs and tissues was normal with no treatment-related changes observed. No significant alterations were found in hemoglobin concentration, microhematocrit, total leukocyte counts, reticulocyte counts, serum glutamic-pyruvic and glutamic-oxaloacetic transaminase activities, liver alkaline phosphatase activity, or liver lactate concentrations. In addition, we have delivered DMSO (ca. 10 wt %) in a dry powder formulation with trehalose and L-leucine at a ratio of 78/22 to dogs for 5 consecutive days using a dosing protocol and lung deposition comparative to delivery of 5-AZA (data not included). DMSO inhalation showed no adverse effects with respect to lung histopathology, hematology, or serum biomarkers that address kidney and liver function, electrolyte balance, and metabolic status.

Process Design and Modeling. To understand the drying and expected core-shell architecture of this formulation and process, we developed a DMSO:water:solids ternary phase diagram using PC-SAFT with processing conditions from batch 92-1 (Figure 5). Reference Tables S5 and S6 in the Supporting Information for the PC-SAFT pure component and binary interaction parameters used in this model. The spray solution for batch 92-1 (solids composition of 10/20/70 5-AZA/L-leucine/trehalose at 5 wt % solids loading in 90/10 DMSO/water) is depicted by the blue circle. Figure 5 is quantitatively accurate only for a constant ratio of 5-AZA/Lleucine/trehalose (10/20/70) and at 70 °C (target spraydrying outlet temperature). As the droplet dries, L-leucine crystallizes, and therefore the ratio of 5-AZA/L-leucine/ trehalose changes in the liquid/amorphous phase during the drying process. Additionally, the temperature of the droplet varies during drying due to evaporative cooling and changes in the evaporation rate as the L-leucine shell solidifies. Therefore, once drying has commenced, Figure 5 is no longer quantitatively accurate; however, it is useful in qualitatively understanding the droplet drying process.

Upon contact with the drying gas, the droplet begins to dry and move along the drying trajectory (Figure 5, blue line), with water evaporating faster than DMSO due to higher relative volatility. ^{25,45} Upon crossing the solubility limit of L-leucine (first solid orange line), phase separation occurs and as a rapid crystallizer, L-leucine shell formation is spontaneously initiated. ^{14,19} The L-leucine shell forms rapidly, reaching equilibrium early in droplet drying, while molecular mobility is sufficiently high. As the particle continues to dry, the drying trajectory crosses the trehalose solubility limit; however, trehalose is not a rapid crystallizer relative to L-leucine, and therefore, the short drying time scale prevents in situ crystallization of trehalose. This is further supported by XRD (Figure 2), which does not show crystalline trehalose in the spray-dried powders. As drying continues, DMSO begins to accumulate in the particle, increasing the driving force for

evaporation and leading to improved drying. Toward the end of the drying trajectory, the shell is more solidified, and the $T_{\rm g}$ of the core has increased due to solvent removal, which kinetically inhibits further solvent evaporation.

Droplet drying is predicted to end beyond the 5-AZA solubility limit (Figure 5, green X). The 5-AZA solubility limit is depicted as a banded region rather than a line in Figure 5 because the solubility of 5-AZA changes as a function of composition, and the composition is changing as the droplet dries. In the beginning of droplet drying (where Figure 5 is quantitatively accurate with a droplet composition of 10/20/ 70 5-AZA/L-leucine/trehalose, 5 wt % solids loading in 90/10 DMSO/water), the solubility boundary is calculated as the leftmost border of the orange region by PC-SAFT. As drying commences and solvents evaporate, the composition of the droplet changes. Simultaneously, the composition of the core changes as the L-leucine phase separates, migrates to the droplet surface, and forms the shell structure. The exact ratio of amorphous:crystalline L-leucine present in the final powder remains unknown; however, it is hypothesized to be low based on its precedence as a rapid shell former. Molecular mobility is low near the end of drying, and therefore in situ 5-AZA crystallization is unlikely and all 5-AZA is assumed to remain amorphous in the trehalose matrix. Additionally, no crystalline 5-AZA or crystalline trehalose was observed in the powders via XRD (Figure 2). The solubility of 5-AZA with a core composition of 12.5/0/87.5 5-AZA/L-leucine/trehalose is given by the rightmost border of the orange region. During thermal characterization of the manufactured SDPs, 5-AZA crystallization was observed via an enthalpic event following the glass transition (Figure S2 in the Supporting Information). The temperature at which the enthalpic peak was observed varied between formulations but occurred 77 °C beyond the T_g for the 10 wt % control formulation and generally occurred 40° °C-50 °C beyond the T_g for the 20 wt % active loading SDPs. This suggests that following crossing the vitrification boundary (green line), 5-AZA crystallization is not immediate.

To the best of our knowledge, this is the first study of engineering core—shell architectures with L-leucine and trehalose using a DMSO/water solvent system in the spraydrying process. A comparison to the same formulation processed out of ethanol and water (the most precedented system for L-leucine-containing core—shell architectures in the literature) is given by Figure S3 in the Supporting Information. Although the drying trajectories of the two processes appear different due to differences in ethanol and DMSO volatilities relative to water, the trajectories cross solubility boundaries of L-leucine, trehalose, and 5-AZA at similar composition points along the droplet lifecycle. Therefore, similar phase separation, crystallization, and final particle architecture are expected between the ethanol:water:solids and DMSO:water:solids processes.

CONCLUSIONS

In response to a recent study demonstrating inhaled dry powder 5-AZA improves efficacy compared to other dosage forms, we studied the spray-drying process by which the inhaled dry powder was manufactured. We manufactured a series of spray-dried powders with the objective of increasing 5-AZA loading in the formulation and advancing our understanding of both the formulation and process and their impacts on powder properties.

Characterization of the manufactured spray-dried powders matched the particle morphology, size distribution, residual DMSO content, and purity of the powders used in prior work with additional tunability of residual DMSO demonstrated. A core—shell structure similar to that seen in the literature when spray drying L-leucine and trehalose in water and water/ethanol blends was observed here when manufacturing from a DMSO/water blend. The particle size distribution of the powders is suitable for pulmonary delivery.

We successfully spray dried a material with a $T_{\rm g}$ below room temperature (and at least 80 °C below the outlet temperature) with a high yield, attributable to L-leucine in the formulation as a shell former. The results suggest that spray drying with a shell former enables the manufacture of a dry powder with a $T_{\rm g}$ below the spray dryer outlet temperature and even room temperature.

We demonstrated the tunability of the residual DMSO content through process engineering. The residual DMSO content was found to be controlled primarily by the DMSO/ water ratio and, to a lesser extent, the 5-AZA/trehalose ratio in the core. As mentioned previously, a primary objective of this work was to match powder properties (including DMSO content) of the previous in vivo study, which was successful. Control of the residual DMSO content in the manufactured powders may be important for further optimization of stability and exposure to DMSO in the lung.

Modeling is important in process design and the scale up of complex processes and formulations. PC-SAFT was employed to understand the droplet drying process by developing ternary phase diagrams and drying trajectories. These models informed our understanding of the core—shell architecture, the mechanism by which it was formed, and the composition of the core as a function of the drying progress. The use of PC-SAFT is increasingly important, as more active molecules require multiple solvents for solubilization and spray dry processing.

The findings from this work enable and inform the manufacture and scale-up of both dry inhalable 5-AZA powders for the treatment of lung cancer and low $T_{\rm g}$ materials previously thought to be unmanufacturable by spray drying. This work has implications for allowing the spray drying of low $T_{\rm g}$ compositions for other applications and delivery modalities, including oral dosage forms. Additionally, this work highlights the importance of aligning experimental data and theoretical models to improve the fundamental understanding of complex processes.

ASSOCIATED CONTENT

Supporting Information

The Supporting Information is available free of charge at https://pubs.acs.org/doi/10.1021/acs.molpharmaceut.5c00799.

Spray-drying manufacturing summary, GC method details, HPLC gradient method details, physicochemical properties of materials, additional SEM and XRD data, parameters used in the PC-SAFT model, and additional ternary phase diagram (PDF)

AUTHOR INFORMATION

Corresponding Author

Michael E. Grass — Bend Bioscience, Bend, Oregon 97701, United States; o orcid.org/0000-0002-1567-7271; Email: Michael.Grass@BendBioscience.com

Authors

Rebekah M. Anderson – Bend Bioscience, Bend, Oregon 97701, United States; oorcid.org/0000-0001-6376-6896

Steven A. Belinsky – Lovelace Biomedical Research Institute, Albuquerque, New Mexico 87108, United States

Lindsey M. Earnest – Bend Bioscience, Bend, Oregon 97701, United States

Philip J. Kuehl – Lovelace Biomedical Research Institute, Albuquerque, New Mexico 87108, United States; orcid.org/0000-0002-7567-3002

Christian Luebbert — Amofor GmbH, Dortmund 44227, Germany; o orcid.org/0000-0001-5555-4965

Conor A. Ruzycki – Lovelace Biomedical Research Institute, Albuquerque, New Mexico 87108, United States

David T. Vodak – Bend Bioscience, Bend, Oregon 97701, United States

Complete contact information is available at: https://pubs.acs.org/10.1021/acs.molpharmaceut.5c00799

Notes

ī

The authors declare no competing financial interest.

ACKNOWLEDGMENTS

We would like to acknowledge Lovelace Biomedical for financial internal research and development support. We would also like to acknowledge Kurt Langworthy of CAMCOR and the use of University of Oregon's CAMCOR materials characterization facility for acquiring the SEM images.

REFERENCES

- (1) Jones, P. A.; Baylin, S. B. The Fundamental Role of Epigenetic Events in Cancer. *Nat. Rev. Genet.* **2002**, *3*, 415–428.
- (2) Herman, J. G.; Baylin, S. B. Gene Silencing in Cancer in Association with Promoter Hypermethylation. *N. Engl. J. Med.* **2003**, 349 (21), 2042–2054.
- (3) Christman, J. K. 5-Azacytidine and 5-Aza-2'deoxycytidine as Inhibitors of DNA Methylation: Mechanistic Studies and Their Implications for Cancer Therapy. *Oncogene* **2002**, *21*, 5483–5495.
- (4) Cancer Genome Atlas Research Network. Comprehensive Molecular Profiling of Lung Adenocarcinoma. *Nature* **2014**, *511* (7511), 543–550.
- (5) Juergens, R. A.; Wrangle, J.; Vendetti, F. P.; Murphy, S. C.; Zhao, M.; Coleman, B.; Sebree, R.; Rodgers, K.; Hooker, C. M.; Franco, N.; Lee, B.; Tsai, S.; Delgado, I. E.; Rudek, M. A.; Belinsky, S. A.; Herman, J. G.; Baylin, S. B.; Brock, M. V.; Rudin, C. M. Combination Epigenetic Therapy Has Efficacy in Patients with Refractory Advanced Non-Small Cell Lung Cancer. *Cancer Discovery* **2011**, *1* (7), 598–607.
- (6) Garcia-Manero, G.; Gore, S. D.; Cogle, C.; Ward, R.; Shi, T.; MacBeth, K. J.; Laille, E.; Giordano, H.; Sakoian, S.; Jabbour, E.; Kantarjian, H.; Skikne, B. Phase I Study of Oral Azacitidine in Myelodysplastic Syndromes, Chronic Myelomonocytic Leukemia, and Acute Myeloid Leukemia. *J. Clin. Oncol.* **2011**, 29 (18), 2521–2527.
- (7) Savona, M. R.; Kolibaba, K.; Conkling, P.; Kingsley, E. C.; Becerra, C.; Morris, J. C.; Rifkin, R. M.; Laille, E.; Kellerman, A.; Ukrainskyj, S. M.; Dong, Q.; Skikne, B. S. Extended Dosing with CC-486 (Oral Azacitidine) in Patients with Myeloid Malignancies. *Am. J. Hematol.* **2018**, 93 (10), 1199–1206.

- (8) Kuehl, P. J.; Tellez, C. S.; Grimes, M. J.; March, T. H.; Tessema, M.; Revelli, D. A.; Mallis, L. M.; Dye, W. W.; Sniegowski, T.; Badenoch, A.; Burke, M.; Dubose, D.; Vodak, D. T.; Picchi, M. A.; Belinsky, S. A. 5-Azacytidine Inhaled Dry Powder Formulation Profoundly Improves Pharmacokinetics and Efficacy for Lung Cancer Therapy through Genome Reprogramming. *Br. J. Cancer* **2020**, *122* (8), 1194–1204.
- (9) Lipworth, B. New Perspectives on Inhaled Drug Delivery and Systemic Bioactivity. *Thorax* **1995**, *50*, 105–110.
- (10) Nguyen-Kim, T. D. L.; Frauenfelder, T.; Strobel, K.; Veit-Haibach, P.; Huellner, M. W. Assessment of Bronchial and Pulmonary Blood Supply in Non-Small Cell Lung Cancer Subtypes Using Computed Tomography Perfusion. *Invest. Radiol.* **2015**, *50* (3), 179–186.
- (11) Pilcer, G.; Amighi, K. Formulation Strategy and Use of Excipients in Pulmonary Drug Delivery. *Int. J. Pharm.* **2010**, 392 (1–2). 1–19.
- (12) Weers, J. G.; Tarara, T. E.; Clark, A. R. Design of Fine Particles for Pulmonary Drug Delivery. *Expert Opin. Drug Delivery* **2007**, *4* (3), 297–313.
- (13) Dabbagh, A.; Abu Kasim, N. H.; Yeong, C. H.; Wong, T. W.; Abdul Rahman, N. Critical Parameters for Particle-Based Pulmonary Delivery of Chemotherapeutics. *J. Aerosol Med. Pulm. Drug Delivery* **2018**, *31*, 139–154.
- (14) Ordoubadi, M.; Gregson, F. K. A.; Wang, H.; Nicholas, M.; Gracin, S.; Lechuga-Ballesteros, D.; Reid, J. P.; Finlay, W. H.; Vehring, R. On the Particle Formation of Leucine in Spray Drying of Inhalable Microparticles. *Int. J. Pharm.* **2021**, *592*, 120102.
- (15) Boraey, M. A.; Hoe, S.; Sharif, H.; Miller, D. P.; Lechuga-Ballesteros, D.; Vehring, R. Improvement of the Dispersibility of Spray-Dried Budesonide Powders Using Leucine in an Ethanol-Water Cosolvent System. *Powder Technol.* **2013**, 236, 171–178.
- (16) Alhajj, N.; O'Reilly, N. J.; Cathcart, H. Leucine as an Excipient in Spray Dried Powder for Inhalation. *Drug Discovery Today* **2021**, *26*, 2384–2396.
- (17) Vehring, R. Pharmaceutical Particle Engineering via Spray Drying. *Pharm. Res.* **2008**, *25*, 999–1022.
- (18) Chew, N. Y. K.; Tang, P.; Chan, H.-K.; Raper, J. A. How Much Particle Surface Corrugation Is Sufficient to Improve Aerosol Performance of Powders? *Pharm. Res.* **2005**, 22 (1), 148–152.
- (19) Feng, A. L.; Boraey, M. A.; Gwin, M. A.; Finlay, P. R.; Kuehl, P. J.; Vehring, R. Mechanistic Models Facilitate Efficient Development of Leucine Containing Microparticles for Pulmonary Drug Delivery. *Int. J. Pharm.* **2011**, 409 (1–2), 156–163.
- (20) Zillen, D.; Beugeling, M.; Hinrichs, W. L. J.; Frijlink, H. W.; Grasmeijer, F. Natural and Bioinspired Excipients for Dry Powder Inhalation Formulations. *Curr. Opin. Colloid Interface Sci.* **2021**, *56*, 101497.
- (21) Balouzet, C.; Chanat, C.; Jobard, M.; Brandely-Piat, M.; Chast, F. Stability of 25 Mg/ML Azacitidine Suspensions Kept in Fridge after Freezing. *Pharm. Technol. Hosp. Pharm.* **2017**, 2 (1), 11–16.
- (22) Sun, H.; Du, C. Dissolution of 5-Azacytidine in Aqueous Solution of Alcohols at Various Temperatures: Preferential Solvation and Thermodynamic Analysis. *J. Chem. Thermodyn.* **2023**, *178*, 106945.
- (23) Belinsky, S. A., Kuehl, P. J., Badenoch, A., Burke, M., Dubose, D. Inhalable Dry Powder Cytidine Analogue Composition and Method of Use as a Treatment for Cancer. U.S. Patent 11,266,599 B2, 2022; Vol. 11, p 266.
- (24) Luebbert, C.; Real, D.; Sadowski, G. Choosing Appropriate Solvents for ASD Preparation. *Mol. Pharmaceutics* **2018**, *15* (11), 5397–5409.
- (25) Dohrn, S.; Reimer, P.; Luebbert, C.; Lehmkemper, K.; Kyeremateng, S. O.; Degenhardt, M.; Sadowski, G. Thermodynamic Modeling of Solvent-Impact on Phase Separation in Amorphous Solid Dispersions during Drying. *Mol. Pharm.* **2020**, *17* (7), 2721–2733.
- (26) Dohrn, S.; Rawal, P.; Luebbert, C.; Lehmkemper, K.; Kyeremateng, S. O.; Degenhardt, M.; Sadowski, G. Predicting Process

- Design Spaces for Spray Drying Amorphous Solid Dispersions. *Int. J. Pharm.:X* **2021**, *3*, 100072.
- (27) Gross, J.; Sadowski, G. Perturbed-Chain SAFT: An Equation of State Based on a Perturbation Theory for Chain Molecules. *Ind. Eng. Chem. Res.* **2001**, 40 (4), 1244–1260.
- (28) Chatterji, D. C.; Gallelli, J. F. Stabilization of 5-azacytidine by Nucleophilic Addition of Bisulfite Ion. *J. Pharm. Sci.* **1979**, *68* (7), 822–826.
- (29) Moura, C.; Campos, S.; Neves, F.; Aguiar-Ricardo, A.; Costa, E. Manipulation of Spray-Dried Composite Particles Physiochemical Properties and In-Vitro Performance. *J. Aerosol Med. Pulm. Drug Delivery* **2016**, 29, A9.
- (30) Ordoubadi, M.; Shepard, K. B.; Wang, H.; Wang, Z.; Pluntze, A. M.; Churchman, J. P.; Vehring, R. On the Physical Stability of Leucine-Containing Spray-Dried Powders for Respiratory Drug Delivery. *Pharmaceutics* **2023**, *15* (2), 435.
- (31) Mangal, S.; Meiser, F.; Tan, G.; Gengenbach, T.; Denman, J.; Rowles, M. R.; Larson, I.; Morton, D. A. V. Relationship between Surface Concentration of L-Leucine and Bulk Powder Properties in Spray Dried Formulations. *Eur. J. Pharm. Biopharm.* **2015**, *94*, 160–169
- (32) Zhang, C.; van de Weert, M.; Bjerregaard, S.; Rantanen, J.; Yang, M. Leucine as a Moisture-Protective Excipient in Spray-Dried Protein/Trehalose Formulation. *J. Pharm. Sci.* **2024**, *113* (113), 2764–2774.
- (33) Sou, T.; Kaminskas, L. M.; Nguyen, T. H.; Carlberg, R.; McIntosh, M. P.; Morton, D. A. V. The Effect of Amino Acid Excipients on Morphology and Solid-State Properties of Multi-Component Spray-Dried Formulations for Pulmonary Delivery of Biomacromolecules. *Eur. J. Pharm. Biopharm.* **2013**, *83* (2), 234–243.
- (34) Hassan, A.; Farkas, D.; Longest, W.; Hindle, M. Characterization of Excipient Enhanced Growth (EEG) Tobramycin Dry Powder Aerosol Formulations. *Int. J. Pharm.* **2020**, *591*, 120027.
- (35) Lamy, B.; Remedios Serrano, D.; O'connell, P.; Couet, W.; Marchand, S.; Healy, A. M.; Tewes, F. Use of Leucine to Improve Aerodynamic Properties of Ciprofloxacin-Loaded Maltose Microparticles for Inhalation. *Eur. . Pharm. Res.* **2019**, *1* (1), 2–11.
- (36) Downton, G. E.; Flores-Luna, J. L.; King, C. J. Mechanism of Stickiness in Hygroscopic, Amorphous Powders. *Ind. Eng. Chem. Fundam.* **1982**, *21* (4), 447–451.
- (37) Bhandari, B. R.; Datta, N.; Howes, T. Problems Associated With Spray Drying of Sugar-Rich Foods. *Drying Technol.* **1997**, *15* (2), 671–684.
- (38) Du, J.; Ge, Z.-Z.; Xu, Z.; Zou, B.; Zhang, Y.; Li, C.-M. Comparison of the Efficiency of Five Different Drying Carriers on the Spray Drying of Persimmon Pulp Powders. *Drying Technol.* **2014**, *32*, 1157–1166.
- (39) Fazaeli, M.; Emam-Djomeh, Z.; Kalbasi Ashtari, A.; Omid, M. Effect of Spray Drying Conditions and Feed Composition on the Physical Properties of Black Mulberry Juice Powder. *Food Bioprod. Process.* **2012**, *90* (4), *667–675*.
- (40) Masters, K. Spray-Air Contact (Mixing and Flow). In *Spray Drying Handbook*; Masters, K., Ed.; Halsted Press: New York, 1979; pp 286–290.
- (41) Muzaffar, K.; Nayik, G. A.; Kumar, P. Stickiness Problem Associated with Spray Drying of Sugar and Acid Rich Foods: A Mini Review. *J. Nutr. Food Sci.* **2015**, S12:003.
- (42) Rezvankhah, A.; Emam-Djomeh, Z.; Askari, G. Encapsulation and Delivery of Bioactive Compounds Using Spray and Freeze-Drying Techniques: A Review. *Drying Technol.* **2019**, *38*, 235–258.
- (43) Quek, S. Y.; Chok, N. K.; Swedlund, P. The Physicochemical Properties of Spray-Dried Watermelon Powders. *Chem. Eng. Process.* **2007**, *46*, 386–392.
- (44) Fishman, E. G.; Jenkins, L. J.; Coon, R. A.; Jones, R. A. Effects of Acute and Repeated Inhalation of Dimethyl Sulfoxide in Rats. *Toxicol. Appl. Pharmacol.* **1969**, *15*, 74–82.
- (45) Dohrn, S.; Luebbert, C.; Lehmkemper, K.; Kyeremateng, S. O.; Degenhardt, M.; Sadowski, G. Solvent Influence on the Phase

Behavior and Glass Transition of Amorphous Solid Dispersions. *Eur. J. Pharm. Biopharm.* **2021**, *158*, 132–142.

